

Digital Linear Chirp Receiver for High Chirp Rates With High Resolution Time-of-Arrival and Time-of-Departure Estimation

STEPHEN BENSON
CHIEN-IN H. CHEN
Wright State University
Dayton, OH, USA

DAVID M. LIN
LIHYEH L. LIOU
Air Force Research Laboratory
Wright Patterson AFB, OH, USA

The use of chirp signals in modern radar and ranging systems have numerous benefits. They are extensively used to improve signal-to-noise ratio and range resolution. The performance capabilities of these signals are directly related to their time-bandwidth product, i.e., the duration and bandwidth of the pulse. Ultra-wideband chirp signals are further desirable because they span a large bandwidth, making them resistant to narrowband environmental interference. The accurate detection and measurement of high chirp signals is difficult due to the necessity of a high-sampling analog-digital converter, a target measurement platform with high computational power, and a time-of-arrival (TOA) estimator with high temporal resolution. The difficulty of the problem is further compounded with the requirement that no a priori knowledge of the signal, noise, or operating environment is known. This paper presents a practical approach and implementation of a high linear chirp rate receiver and TOA estimator pair capable of detecting and measuring stationary radio frequency pulses as well as linear chirp rates up to 1.18 GHz in 400 ns. The high-resolution TOA algorithm and linear chirp receiver have been prototyped, synthesized, and placed and routed for a Virtex 6 SX475 FPGA.

Manuscript received September 2, 2014; revised March 1, 2015, August 4, 2015; released for publication November 4, 2015.

DOI. No. 10.1109/TAES.2016.140656.

Refereeing of this contribution was handled by P. Pace.

Authors' address: Wright State University, Electrical Engineering, 3640 Colonel Glenn Highway, Dayton, Ohio 45435 USA. Corresponding author is C.-I. H. Chen, E-mail: (henry.chen@wright.edu).

0018-9251/16/\$26.00 © 2016 IEEE

I. INTRODUCTION

A chirp signal is defined as a signal whose frequency changes over a period of time. Chirp signals are becoming ever more present in many current applications and technologies. Some of their applications include measuring the thickness of snow over sea ice [1], automotive radar ranging applications [2], multifunctional communications and radar systems [3], and multiple input/multiple output radars [4]. One of the most desirable qualities of chirp signals is their ability to resolve targets with high range resolution without sacrificing pulse duration. The maximal range resolution of a chirp signal is defined by

$$\text{Range Resolution} = \frac{c}{2 * \text{BW}}, \quad (1)$$

where c is the speed of the wave, and BW is the bandwidth of the transmitted signal. Chirp signals also have other desirable qualities, including resistance to narrowband interference as well as improved signal-to-noise ratio (SNR) when utilized with pulse compression techniques. Chirp signals can be classified as either linear or nonlinear. If the chirp rate is small relative to the measurement period, a traditional instantaneous frequency measurement (IFM) or fast Fourier transform (FFT) can be used over multiple measurement periods to estimate the chirp rate through slope calculation. However, this method is impractical for use with high chirp rates that change significantly in a single measurement period. Chirp rates can be classified as up or down chirps, i.e., the frequency can increase or decrease over time. The research presented in this paper focuses on up chirps; however, the techniques used are also practical for use with down chirps.

Wigner distribution has been used to detect nonstationary phase-modulated signals [5, 6]. By computing the line integral of the Wigner distribution of linear frequency-modulated signal along all lines in the time-frequency plane, it is found that the line that produces the maximum value corresponds to the maximum likelihood of the linear instantaneous frequency of the chirp. The Radon-Wigner transform [7] convert the problem of tracking straight lines in the time-frequency plane into locating maxima in an initial frequency versus chirp rate two-dimensional plane. Radon-ambiguity transform [8] combines the Radon-Wigner transform and the ambiguity function to improve the detection of linear frequency-modulated signals by searching the location of maxima over chirp rates only. Another approach using fractional autocorrelation for parameter estimation of linear frequency-modulated signal and chirp rate was proposed [9]. The Hough transform (HT) was proposed to reduce computational load to detect long and very slow chirp signal, i.e., 1-Hz drop in a 10-h interval [10]. Mathematical models proposed by these approaches require large computation. No hardware implementation or chirp rate range was discussed or tested.

The receiver proposed in this research is targeted for real-time unknown signal interception that includes the

detection of stationary (nonchirp) signals or linear frequency-modulated signals. The receiver utilizes a short measurement period of only 100 ns to allow for the measurement of short pulses with high pulse repetition frequencies. The receiver is capable of measuring linear chirp rates between 50 MHz in 400 ns up to 1180 MHz in 400 ns with starting frequencies ranging from 50 up to 1180 MHz. Intuitively, the starting frequency combined with the chirp rate cannot surpass half of the sampling rate (2.56 GHz) within 400 ns. A limitation of this receiver is that pulsed waveform (PW) linear chirp signals must have a pulse width of 400 ns due to the receiver's inability to adjust internal delay values. The internal delay values are optimized for chirp periods of 400 ns. The minimum pulse repetition interval (PRI) for the receiver is 500 ns. There are currently no real-time commercial solutions available that can detect and measure signals that span such a large bandwidth in such a short amount of time [11].

The receiver is also capable of measuring nonchirp (stationary) PWs with carrier frequencies ranging from 50 up to 1230 MHz. Stationary PWs are only required to have a minimum pulse width of 400 ns because the receiver's internal delay values do not affect the carrier frequency measurement of stationary signals.

The digital linear chirp receiver is intended for real-time implementation on readily available field-programmable gate arrays (FPGAs). For this reason, a digital IFM, which was previously developed in [12] and discussed in depth in [13], was chosen as the foundation for frequency measurement within the receiver. The digital IFM's small hardware footprint and high measurement accuracy makes it the ideal foundation for the receiver. Utilizing only 256 samples (100 ns), the digital IFM is capable of a frequency measurement resolution of 1 MHz. To achieve a near equal resolution from an FFT would require a 4096 point (1.6 μ s) FFT.

A consequence of utilizing a digital IFM within the receiver is that the detection of multiple simultaneous signals is not possible. Additional details of the operation and evolution of the IFM is provided in [14], and a comparison of the digital IFM with an analog IFM design is given in [15].

Other previous work relevant to the digital linear chirp receiver includes the implementation of a HT [16]. Both the digital IFM and HT have been tested and verified on a Xilinx Virtex-4 SX55 FPGA utilizing a sampling rate of 2.56 GHz. A brief linear chirp receiver without time-of-arrival (TOA) estimation was previously examined in [17].

This paper will begin by covering the necessary steps to measure the chirp rate and starting frequency of a linear chirp signal, including a mathematical decomposition. Next, the receiver's TOA estimation process will be discussed, including its development and functionality. Further details regarding the operation of the digital linear chirp receiver, including the HT, digital IFM, and dechirping block will then be covered. Finally, the digital linear chirp receiver's performance will be quantified

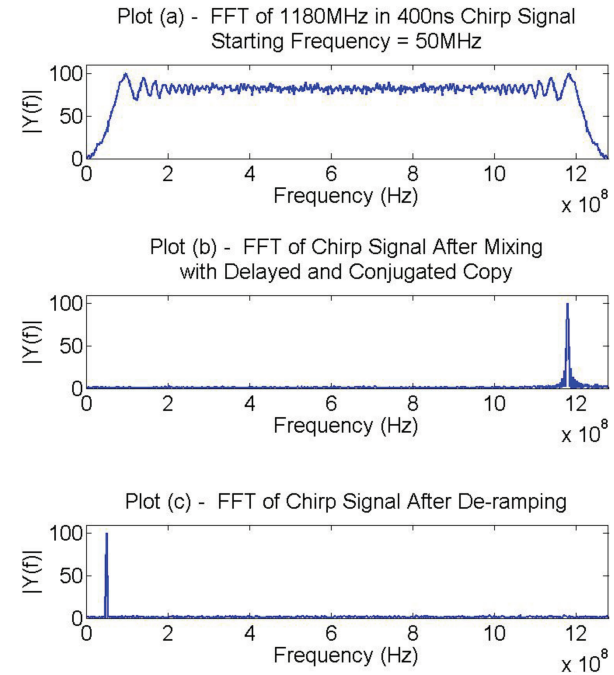


Fig. 1. (a) FFT spectrum of linear chirp signal with chirp rate of 1180 MHz in 400 ns and starting frequency of 50 MHz. (b) FFT spectrum of signal after it has been mixed with conjugated and delayed copy of itself. (c) FFT spectrum of chirp signal after it has been mixed with dechirping signal.

and hardware resource utilization figures will be provided.

II. Linear Chirp Rate and Starting Frequency Estimation

Measuring the chirp rate and starting frequency of a linear chirp signal is a multistep process. First, the chirp rate must be measured and removed from the original signal before the starting frequency can be measured. Once the chirp rate has been removed, it becomes simple to measure the carrier frequency (starting frequency) of the signal. For example, the FFT plot of a chirp signal with a chirp rate of 1180 MHz in 400 ns and a starting frequency of 50 MHz is shown in Fig. 1a. If the original signal is elementwise multiplied (mixed) with a delayed and conjugated copy of itself, the chirp rate can be isolated from the carrier frequency. The optimal delay for this process is calculated by subtracting the measurement period from the pulse width of the signal. An FFT plot of the chirp rate isolation is shown in Fig. 1b.

A dechirping signal with an equal and negated ramp rate can then be mixed with the original signal to remove the chirp rate, leaving only the starting frequency, as shown by the FFT spectrum in Fig. 1c. This is the basic principle used to operate the linear chirp receiver.

A detailed mathematical analysis will be discussed to give further insight into the chirp measurement and dechirping process. A mathematical analysis was also previously carried out in [17].

If the original signal is a linear chirp signal, i.e., a signal whose frequency changes linearly with time, then

the digitized signal can be represented by

$$x(n\Delta t) = ae^{j(\omega n\Delta t + (\frac{1}{2})\alpha n^2 \Delta t^2 + \theta)}. \quad (2)$$

In this representation, n is the sample number, ω is the carrier frequency of the signal, α is the chirp rate, a is the amplitude of the signal that is assumed to remain constant, and Δt is the sampling interval.

A delayed version of the signals complex conjugate can be represented by

$$\begin{aligned} x((n-m)\Delta t)' \\ = a'e^{-j(\omega(n-m)\Delta t + (\frac{1}{2})\alpha(n-m)^2 \Delta t^2 + \theta)}. \end{aligned} \quad (3)$$

Mixing the original signal with its delayed complex conjugate therefore becomes

$$\begin{aligned} S_n = ae^{j(\omega n\Delta t + (\frac{1}{2})\alpha n^2 \Delta t^2 + \theta)} \\ * a'e^{-j(\omega(n-m)\Delta t + (\frac{1}{2})\alpha(n-m)^2 \Delta t^2 + \theta)} \\ = a * a' * e^{(j(m\Delta t\omega + \alpha nm\Delta t^2 - 0.5am^2\Delta t^2))}. \end{aligned} \quad (4)$$

In (4), $m\Delta t$ represents m samples of delay. Therefore, if we let

$$\theta_0 = m\Delta t\omega - 0.5\alpha m^2 \Delta t^2 \quad (5)$$

$$\omega_a = \alpha m \Delta t, \quad (6)$$

then θ_0 is constant because m and Δt are constant and the carrier frequency ω and chirp rate α will also not vary during the measurement period, and thus can be considered constants as well. Therefore, ω_a is also constant for a linear chirp rate, and a new signal S_n can be rewritten as follows:

$$S_n = |a|^2 e^{j(\theta_0 + \omega_a n \Delta t)}. \quad (7)$$

Equation (7) represents a PW signal with a carrier frequency ω_a ; if ω_a can be measured, then the chirp rate α can be derived from the following:

$$\alpha = \frac{\omega_a}{m \Delta t}. \quad (8)$$

Because ω_a can be measured using a digital IFM, therefore, α can be derived. Once α has been measured, a new sequence can be generated:

$$D_n = e^{-j((\frac{1}{2})\alpha n^2 \Delta t^2)}. \quad (9)$$

The original signal (2) can now be dechirped by mixing it with the dechirping signal (9). The dechirped signal then becomes:

$$\begin{aligned} F_n = ae^{j(\omega n\Delta t + (\frac{1}{2})\alpha n^2 \Delta t^2 + \theta)} * e^{-j((\frac{1}{2})\alpha n^2 \Delta t^2)} \\ = \alpha e^{j(\omega n\Delta t + \theta)}. \end{aligned} \quad (10)$$

The resulting signal no longer contains a linear chirp rate. The carrier frequency of the stationary PW signal in (10) can be measured by a second digital IFM.

III. TOA ALGORITHM DEVELOPMENT

A. Motivation

Accurate TOA estimation for very high chirp rates is of paramount importance. The digital linear chirp receiver presented in this paper is targeted to measure linear chirp rates up to 1180 MHz in 400 ns based on a sampling rate of 2.56 GHz. At this chirp rate, the carrier frequency changes at a rate of 1.15 MHz every sample. The starting frequency measurement performance of the receiver is therefore heavily dependent on the accuracy of the TOA estimation.

For the original digital IFM design, which only considered stationary PWs, TOA estimation was significantly simpler for many reasons. First, the IFM utilized a simple power estimation calculated over the measurement period of 100 ns in order to detect the presence of a signal. Because incoming signals were stationary, there is no disadvantage to detecting a signal late. If a signal is missed in one measurement period but detected in the second measurement period, the accuracy of the measurement was not affected.

The methodology for signal detection used by the original digital IFM is ineffective for TOA detection of high chirp rate chirp signals. This is because the best possible resolution achievable by the original method is 100 ns. At this resolution, attempting to measure a signal with a chirp rate of 1180 MHz in 400 ns could result in a starting frequency measurement error of roughly 295 MHz. For this reason, a TOA temporal resolution of 100 ns is not sufficient enough to allow for an accurate starting frequency measurement of chirp signals with high linear chirp rates.

Therefore, a new TOA methodology was studied and implemented for use with the linear chirp receiver. The requirements for the TOA algorithm are : 1) minimum operating frequency of 320 MHz, 2) accuracy and resolution capabilities less than ~ 10 ns, 3) detection rate higher than 90%, 4) false alarm rate less than 10^{-7} (1 in 10 000 000), 5) functions for SNRs from 5 up to 20 dB, and 6) signal detection based on no a priori knowledge.

B. Initial TOA Algorithm Development Considerations

In order to minimize computational complexity, simple time-domain amplitude-based criteria were selected for TOA detection. Two of the simplest criteria available are mean value and maximum amplitude-based thresholds. Though data for the receiver is sampled at 2.56 GHz, the FPGA is incapable of operating at this frequency. Therefore, incoming data is transformed from a serial data rate to a parallel one. The data is demultiplexed at a 1:8 ratio, allowing for eight samples to be provided at a rate of 320 MHz. For this reason, mean and amplitude values are evaluated for every eight-sample window. Each sample from the analog-to-digital converter (ADC) is represented by four bits, setting an amplitude range of -7 to 7.

One of the most difficult tasks for TOA detection is determining the optimal thresholds that meet all the

requirements. The difficulty of this task is further increased by the extremely long simulation times needed to test the detection rates and false alarm rates for each threshold setting. In order to overcome this hurdle, a statistical model was developed to greatly reduce the simulation time needed to test different threshold combinations. The statistical model is first used to estimate the detection rate and false alarm rate for a given set of thresholds. A TOA model developed within Simulink/Xilinx System Generator (XSG) is then simulated to verify that all requirements are met.

The statistical model was utilized to estimate two performance metrics: detection rates and false alarm rates. Separate processes are used to estimate each of these rates.

C. Estimating Detection Rates and False Alarm Rates

Detection rates are estimated by evaluating the average values and standard deviations of signals embedded in additive white Gaussian noise (AWGN) across a range of carrier frequencies and SNRs. The first step for creating a batch of test signals involves generating 1180 PW signals with carrier frequencies ranging from 50 up to 1230 MHz. The pulse width for every signal is set to 400 ns, and each signal is given a random phase. A set of these signals is generated for each SNR from 5 up to 20 dB. Finally, this process is iterated 10 times, resulting in a total of 188 800 (400 ns) signals, or $1.93 \times \exp(8)$ total samples.

False alarm rates are estimated by evaluating the average values and standard deviations of a channel with only AWGN present. A total of $1.93 \times \exp(8)$ samples of random noise samples were generated in Matlab. The signals and noise were then analyzed to create multiple cumulative distribution functions (cdfs), which could be used to estimate the detection rates and false alarm rates based on different detection criteria and thresholds.

D. TOA Detection Criteria and Threshold Optimizing

For the initial threshold determination, only signal data at an SNR of 5 dB was considered, which represents the worst-case detection scenario. As the SNR is improved, signal detection will improve, while false alarm probability will remain nearly constant. For all subsequent figures and criteria evaluations in this section, all data is presented at an SNR of 5 dB.

The first criteria considered for TOA estimation is the average of the absolute values of an eight-sample window. Using this criteria, a cdf was generated to show the expected detection rates for all possible thresholds and is shown in the top plot of Fig. 2. The bottom plot of Fig. 2 shows the expected false alarm rates for each threshold. The dotted line in the top plot represents the 90% detection rate threshold and the dotted line in the bottom plot represents the 10^{-7} false alarm rate threshold. The plot clearly shows that it is impossible for a single threshold setting to simultaneously meet a 90% detection rate and 10^{-7} false alarm rate.

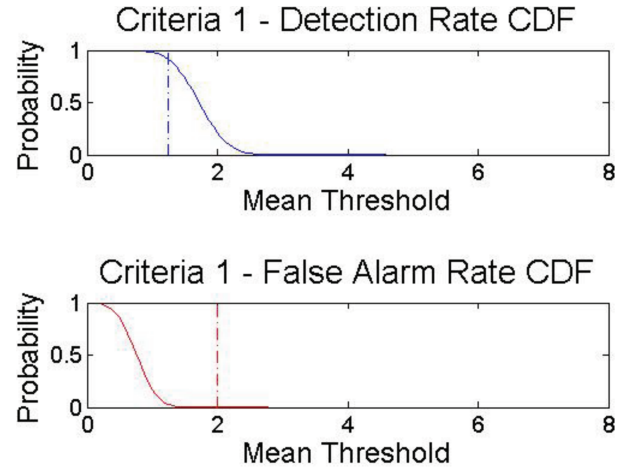


Fig. 2. Detection rate and false alarm rate estimations for mean value threshold setting possibilities of criteria 1. Detection rates are estimated at SNR of 5 dB.

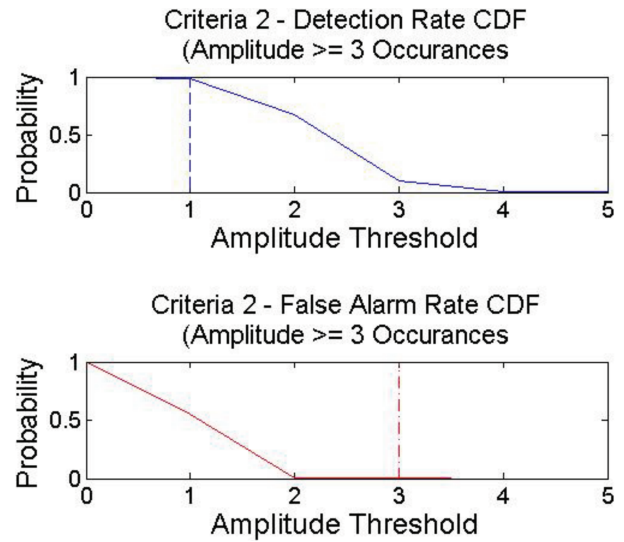


Fig. 3. Detection rate and false alarm rate estimations for magnitude value thresholds that occur at least three times in eight-sample window. Detection rates are estimated at SNR of 5 dB.

The second criteria considered for TOA estimation is the maximum magnitude value encountered within an eight-sample window. For robustness, a second threshold was also added that sets the minimum number of occurrences for a magnitude value within an eight-sample window. After analyzing the data, it was found that magnitude values that occurred at least three times in an eight-sample window achieved the most desirable performance.

Fig. 3 shows the expected detection rates for magnitude values that occur at least three times in an eight-sample window in the top plot. The bottom plot of Fig. 3 shows the expected false alarm rates for magnitude values that occur at least three times in an eight-sample window. The dotted lines represent the 90% detection rate threshold and the 10^{-7} false alarm rate threshold, respectively. The plot once again shows that it is

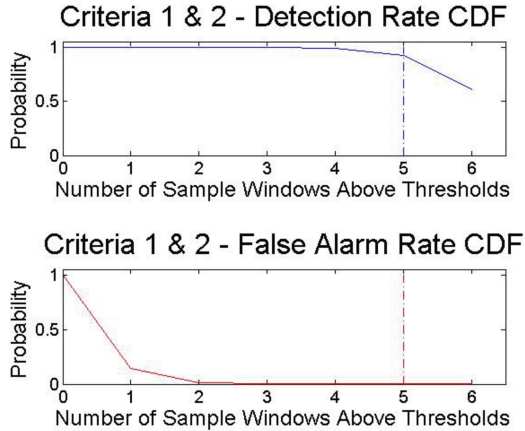


Fig. 4. Detection rate and false alarm rate estimations when criteria 1 and 2 are used simultaneously and evaluated over six-sample windows. Number of required threshold crossings within six-sample windows is plotted on x-axis; y-axis plots probability of detection for top plot and probability of false alarm on bottom plot. Detection rates are estimated at SNR of 5 dB.

impossible for a single threshold setting to simultaneously meet a 90% detection rate and 10^{-7} false alarm rate.

The distributions for all criteria are not assumed to be normally distributed; such is the case with criteria 2, which uses the maximum value within an eight-sample window. However, the distribution for this criteria is assumed to be normal-like because a very large number of samples are utilized and useful estimations are derived from the use of the cdf.

Detection rates and false alarm rates were also estimated when both criteria are utilized simultaneously. For this evaluation, the average threshold for criteria 1 was set to 1.25 and the magnitude threshold for criteria 2 was set to 3 with at least three occurrences in a sample window. Using these thresholds, Fig. 4 shows the estimated detection and false alarm rates based on how many times either threshold is crossed within six sample windows. The dotted line in the top plot represents a 90% detection rate threshold, and the dotted line in the bottom plot represents the 10^{-7} false alarm threshold. Fig. 4 shows that by requiring either of the first two criteria's thresholds to be crossed for at least five sample windows out of six, a 90% detection rate and 10^{-7} false alarm rate can be achieved.

A third criteria was added to increase the robustness and flexibility of the TOA algorithm. The third criteria monitors the average of the absolute values of each eight-sample window over a period of 200 ns (64 sample windows). The third criteria is activated only after either criteria 1 or 2 have been crossed for at least five sample windows out of six. Criteria 3 utilizes two independent thresholds for its operation. The first threshold sets the required average value for the eight-sample windows. The second threshold sets the number of eight-sample windows out of 64 windows (200 ns) that must be above the average threshold.

Fig. 5 shows the threshold combinations that can be chosen that meet at least a 90% detection rate requirement

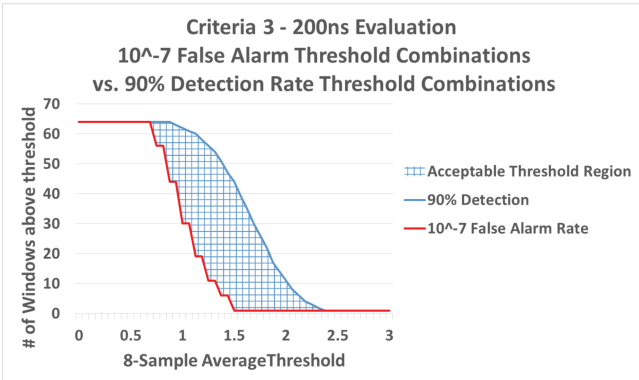


Fig. 5. Depicts number of sample windows out of 64 that are required to meet 90% detection rate or 10^{-7} false alarm rate. Shaded area depicts threshold choices that meet both criteria simultaneously. Detection rates are estimated at SNR of 5 dB.

or a 10^{-7} false alarm rate requirement. The shaded area represents the threshold combinations that satisfy both requirements simultaneously. The x-axis plots the eight-sample average threshold while the y-axis plots the number of sample windows out of 64 that must be above the eight-sample average threshold.

Because the duration of the TOA evaluation period is 70 sample windows, a false alarm rate of 10^{-7} insinuates that a false alarm should occur no more frequently than once every $7.0 \times \exp(7)$ sample windows. In order to meet this new false alarm rate, criteria 3's final average threshold was set to 1, with a minimum number of crossings equal to 42 windows out of 64 windows.

An example PW signal that activates all three criteria has been provided in Fig. 6 to allow for a visualization of the TOA algorithm. The dotted horizontal lines represent the thresholds for each criteria. The vertical dotted lines for criteria 1 and 2 encapsulate six sample windows and the vertical dotted lines in criteria 3 encapsulate 64 sample windows. The figure shows that criteria 1 and 2 operate simultaneously and the signal causes both criteria's thresholds to be crossed for six sample windows. Once this occurs, criteria 3 is activated and evaluated over 64 sample windows (200 ns). Because all sample windows are above criteria 3's average threshold, the signal will be considered detected at the end of the 200-ns evaluation period.

E. Time-of-Departure Detection

Time-of-departure (TOD) is detected using criteria 1 and an independent threshold from the one used for TOA detection. TOD is considered detected when criteria 1's lower threshold is not crossed for at least five sample windows out of six. When a TOD is detected, all detection criteria are reset, regardless of the current state. If criteria 3's thresholds were previously crossed, the TOD information is stored for output by the receiver. If criteria 3's thresholds were not crossed, then the criteria are reset and no information is stored for output.

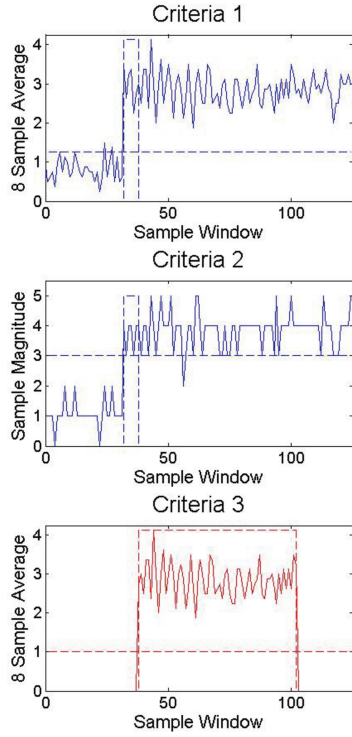


Fig. 6. Example TOA detection of PW signal that activates all three criteria.

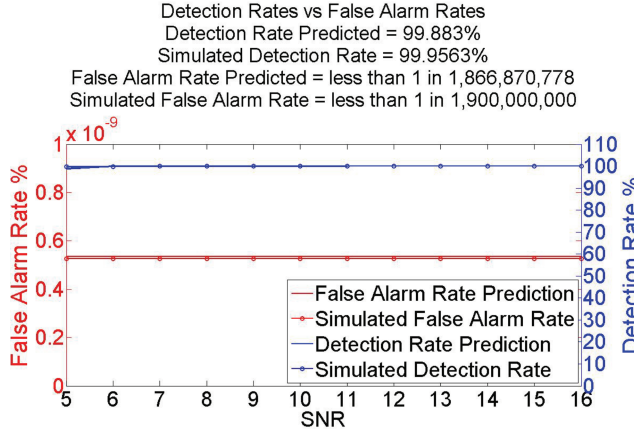


Fig. 7. Detection/false alarm rate estimations and simulated detection/false alarm rates of finalized TOA model.

F. Performance Evaluations

The TOA model in Simulink/XSG was simulated using the final threshold settings in order to verify the estimated performance. It was estimated that the TOA model would achieve an average detection rate of 99.88% for SNRs from 5 to 16 dB with a false alarm rate of 1×10^{-9} sample windows. After simulating the TOA model, it achieved an overall detection rate of 99.95% and a false alarm rate less than 1 in 1.9×10^{-9} sample windows for SNRs between 5 and 16 dB. Fig. 7 shows the final predicted and simulated detection rates and false alarm rates.

A limitation of the statistical model is that it does not predict the temporal accuracy achievable by the TOA

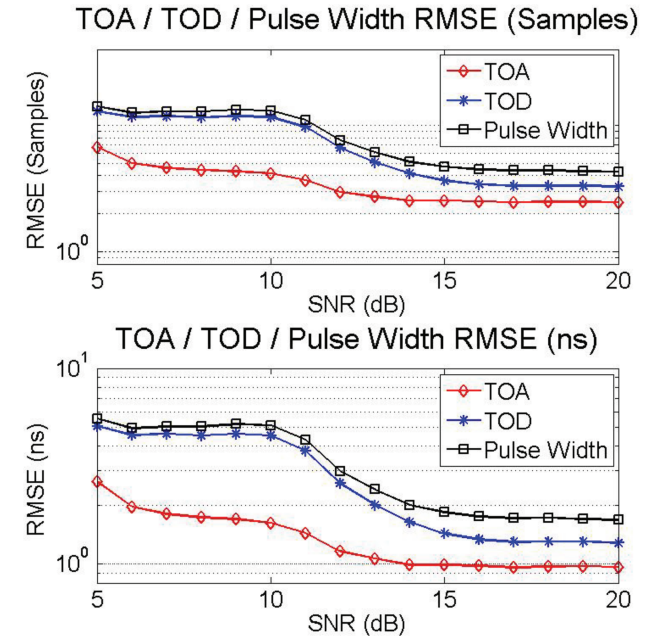


Fig. 8. TOA RMSE, TOD RMSE, and pulse width RMSE for SNRs from 5 up to 20 dB. Each point on graph shows average error obtained from 1130 simulations that simulate linear chirp signal as input. Chirp rate is swept from 50 MHz in 400 ns up to 1180 MHz in 400 ns in 1 MHz increments.

model. Once the thresholds had been finalized, separate simulations were run to test the TOA estimation accuracy. Fig. 8 shows the root-mean-square error (RMSE) TOA error and TOD error pulse width error for SNRs between 5 and 20 dB.

The TOA model achieves an average TOA error of 2.70 samples, an average TOD error of 4.73 samples, and an average pulse width error of 6.30 samples for SNRs from 5 to 20 dB. The high temporal resolution and accuracy of the TOA model is what allows for the detection and measurement of very high chirp rates.

IV. DIGITAL LINEAR CHIRP RECEIVER

A. Data Acquisition and TOA Detection

The ADC being utilized by the receiver is a Calypso 12-bit ADC capable of sampling at 3.6 gigasamples per second (GSPS). The ADC is integrated with a Xilinx Virtex-6 SX475 FPGA. The ADC is configured to sample at 2.56 GSPS and provides four-bit samples of real data to the receiver. The TOA algorithm described in the previous section is used to detect a signal's TOA. Frequency measurement will only begin after the TOA has been detected. To aid in the digital linear chirp receiver design discussion, a data flow chart for the linear chirp receiver can be seen in Fig. 9.

B. HT

Once the TOA has been detected, the incoming data passes through a HT. The HT is necessary to create a complex signal representation of the incoming real data. The digital IFMs used in the design require a complex

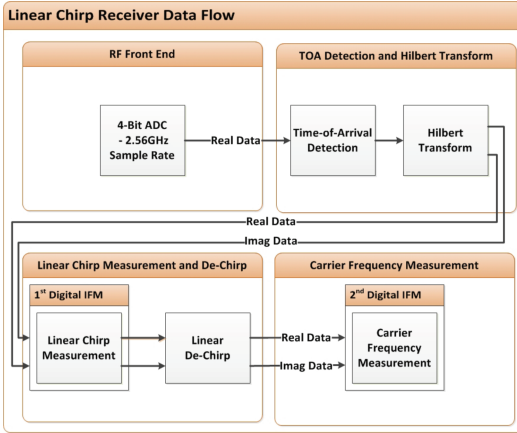


Fig. 9. Hardware flow of digital linear chirp receiver.

signal representation in order to complete a phase measurement. The HT takes a real signal as input, applies a 90° phase shift, which in turn, generates its complex signal representation. A simple HT implementation using a three-tap finite impulse response filter with the coefficients [1 0 -1] was used for the design. The HT functions properly for SNRs of 5 dB or better. Because the TOA estimator is also limited to SNRs of 5 dB or better, the three-tap HT is sufficient for the design.

C. Linear Chirp Rate Measurement

Once the data is transformed into its complex signal representation by HT, the signal is mixed with a delayed and conjugated duplicate of itself. The optimal time delay is determined by subtracting the measurement latency from the pulse width of the signal. The target pulse width for chirp signals presented in this research is 400 ns, and the chosen IFM incurs a latency of 150 ns. The IFM's latency differs from its measurement period of 100 ns. This is due to the autocorrelation operations utilized by the IFM. The longest autocorrelation delay is 50 ns; therefore, the IFM has an initial measurement latency of 150 ns, and all subsequent measurements occur in 100 ns intervals. The IFM operates by collecting 256 complex samples in order to calculate the phase angle and then converts the phase angle into a frequency measurement. More detailed information regarding the operation of the IFM can be found in [12, 13].

Subtracting the latency from the desired chirp period results in an optimal time delay of 250 ns. After the original signal is mixed with its delayed and conjugated copy, the first digital IFM is used to measure the linear chirp rate of the signal, if one is present.

D. Linear Dechirping Process and Carrier Frequency Measurement

If a linear chirp rate is detected, an appropriate dechirping signal is chosen from a dechirping lookup table (LUT). The LUT contains 1024 linear dechirping signals, which are uniformly spaced from 40 MHz in 400 ns up to

1190 MHz in 400 ns. Each dechirping signal is 384 samples long and is represented as a complex signal. The second IFM requires the original signal to be dechirped for 384 samples (150 ns) due to the IFMs initial measurement latency of 150 ns. The dechirping signal is mixed with the original signal to remove the linear chirp rate from the signal. Once the signal has been dechirped, the second IFM is used to measure the carrier frequency.

If no linear chirp rate is present, the original input signal is allowed to pass through without being dechirped; this allows stationary PW signals to be measured as well. The second IFM will continue to measure the carrier frequency of a stationary PW signal every 100 ns until the end of the pulse is detected.

V. DIGITAL LINEAR CHIRP RECEIVER PERFORMANCE EVALUATIONS AND HARDWARE REQUIREMENTS

A. Simulation Parameters

The frequency measurement performance of the linear chirp receiver was measured through Simulink/XSG simulations. The simulations are categorized into two sets. The first set tested the measurement performance of the receiver with linear chirp PW signals, and the second set tested the performance with stationary PW signals. In both sets of simulations, the pulse width of signals was maintained at 400 ns because the PRI was randomly set between 500 and 900 ns. The phase for each signal was randomly assigned, and SNRs were swept from 5 up to 20 dB.

B. Linear Chirp Signal Measurement Performance

Linear chirp signal measurement performance was tested at each SNR ranging from 5 to 20 dB. For each SNR, 1130 chirp signals with chirp rates ranging from 50 MHz in 400 ns up to 1180 MHz in 400 ns were simulated in 1 MHz increments. The carrier frequency for each chirp signal was simultaneously swept from 1180 down to 50 MHz in 1 MHz decrements.

From the simulations, the receiver obtained an average linear chirp measurement error of 0.29 MHz in 400 ns (0.08% error) with a standard deviation of 0.22 MHz in 400 ns. The linear chirp receiver measured the carrier frequency (starting frequency) of linear chirp signals with an average measurement error of 1.7 MHz (0.68% error) and a standard deviation of 1.77 MHz. Fig. 10 shows the RMSE for linear chirp rate and carrier frequency measurements across all simulated SNRs in percent.

C. Stationary Carrier Frequency Measurement Performance

Carrier frequency measurement accuracy of stationary PW signals was tested by measuring 1180 stationary signals at each SNR. The carrier frequency of the signals was swept from 50 up to 1230 MHz in 1 MHz increments. Fig. 11 shows RMSE in percent across all simulated SNRs. The average error was simulated to be 0.26 MHz (0.07% error) with a standard deviation of 0.19 MHz.

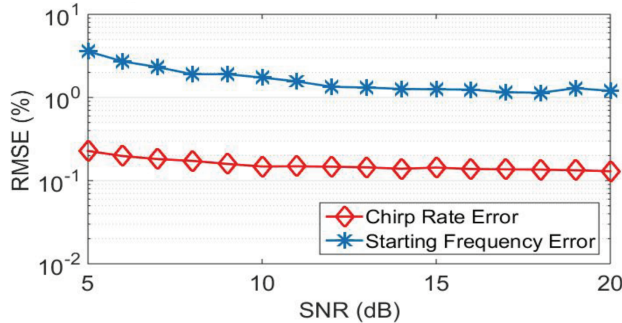


Fig. 10. Linear chirp signal measurement error and carrier frequency measurement error versus SNR.

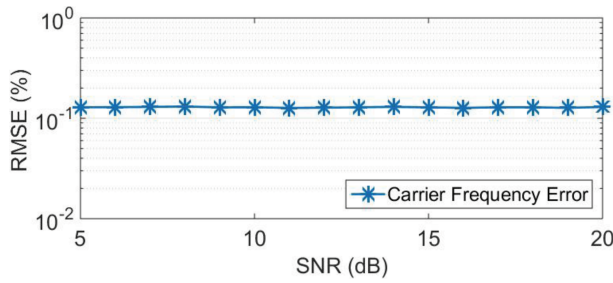


Fig. 11. Carrier frequency measurement error for stationary PWs versus SNR.

TABLE I
Comparison of Chirp Rate and Carrier Frequency Measurement Abilities of Various Receivers

	Linear Chirp Range	Linear Chirp Error
Digital linear chirp receiver	50 MHz in 400 ns–1180 MHz in 400 ns	0.08%
Monobit linear chirp receiver [17]*	80 MHz in 400 ns–1600 MHz in 400 ns	<2%
Digital channelized receiver [18]**	0.4 MHz in 400 ns–4 MHz in 400 ns	1%–10%
	Carrier Range	Carrier Error
Digital linear chirp receiver	50 MHz–1180 MHz	0.68%
Monobit linear chirp receiver [17]	60 MHz–1.2 GHz	<4%
Digital channelized receiver [18]	500 ns pulse–1 μ s pulse	10%

*The original chirp period for the monobit linear chirp receiver was 300 ns. This value was converted to its equivalent chirp in 400 ns for ease of comparison.

**The original chirp period for the digital channelized receiver was 1 μ s. This value was converted to its equivalent chirp in 400 ns for ease of comparison.

D. Relevant Comparisons

Table I compares the results presented in this research with the results obtained from the monobit linear chirp receiver in [17] and the digital channelized receiver in [18]. The digital linear chirp receiver presented in this paper achieves significantly better performance for both linear chirp measurement and carrier frequency measurement of linear chirp signals. It should also be

noted that the monobit linear chirp receiver in [17] assumes perfect TOA detection, whereas TOA is estimated with the digital linear chirp receiver and the digital channelized receiver. This significantly degrades the performance of carrier frequency measurements. Though the chirp rates researched in [18] are significantly slower than the chirp rates presented in this paper, the high linear chirp receiver achieves significantly better measurement results.

TOA estimation results can also be compared with the digital channelized receiver. The digital channelized receiver in [18] utilizes a sampling rate of 250 megasamples per second and has a TOA RMSE of \sim 100 samples at an SNR of 5 dB. At the same SNR, the digital linear chirp receiver achieves a TOA RMSE of 6.73 samples.

E. Hardware Utilization

The digital linear chirp receiver with TOA estimation has been fully synthesized with a completed place and route in Xilinx ISE 13.4. The target FPGA is a Virtex 6 SX475 FPGA, and the hardware utilization is 7% with 24 000 LUTs being used.

VI. CONCLUSION

Modern digital receivers, whether IFM based or FFT based, lack the ability to handle high chirp ultra-wideband (UWB) signals in real-time. This paper successfully demonstrates a proof of concept for a digital UWB high linear chirp rate receiver. The uniqueness of the design is its ability to accurately measure unknown signals that span a large bandwidth in a short pulse duration. An implementation of the design has been executed on a Virtex 6 FPGA. The paper also presents an acceptable TOA algorithm that allows for the detection of short pulses.

One of the most appealing features of this design is its small size and modularity. The TOA algorithm and receiver are easily reconfigurable, allowing for the measurement of different chirp periods, whether significantly slower or faster. Future work will focus on an implementation that can optimize internal delay values dynamically, allowing the receiver to be capable of measuring chirp rates that span a wide range of pulse widths. The ability to detect and measure nonlinear chirp rates will also be studied.

REFERENCES

- [1] Kanagaratnam, P., Markus, T., Lytle, V. I., Heavey, B., Jansen, P. Prescott, G., and Gogineni, S. P. Ultra-wideband radar measurements of thickness of snow over sea ice. *Transactions of Geoscience and Remote Sensing*, **45**, 9 (Sep. 2007), 2715–2724.
- [2] Kronauge, M., and Rohling, H. New chirp sequence radar waveform.

- [3] Saddik, G. N., Singh, R. S., and Brown, R. Ultra-wideband multifunctional communications/radar system. *IEEE Transactions on Microwave Theory and Techniques*, **55**, 7 (Jul. 2007), 1431–1437.
- [4] Wang, W. Q. Large time-bandwidth product MIMO radar waveform design based on chirp rate diversity. *IEEE Sensors Journal*, **15**, 2 (Feb. 2015), 1027–1034.
- [5] Boudreault-Bartels, G. F., and Parks, T. W. Time-varying filtering and signal estimation techniques using Wigner distribution synthesis techniques. *IEEE Transactions on Acoustic, Speech, and Signal Processing*, **34**, 3 (Jun. 1986), 442–451.
- [6] Li, W. Wigner distribution method equivalent to dechirp method for detecting a chirp signal. *IEEE Transactions on Acoustics, Speech, and Signal Processing*, **35**, 8 (Aug. 1987), 1210–1211.
- [7] Wood, J. C., and Barry, D. T. Radon transformation of time-frequency distributions for analysis of multicomponent signals. *IEEE Transactions on Signal Processing*, **42**, 11 (Nov. 1994), 3166–3177.
- [8] Wang, M., Chan, A. K., and Chui, C. K. Linear frequency-modulated signal detection using Radon-ambiguity transform. *IEEE Transactions on Signal Processing*, **46**, 3 (Mar. 1998), 571–585.
- [9] Akay, O., and Boudreault-Bartels, G. F. Fractional convolution and correlation via operator methods and an application to detection of linear FM signals. *IEEE Transactions on Signal Processing*, **49**, 5 (May 2001), 979–993.
- [10] Sun, Y., and Willett, P. Hough transform for long chirp detection. *IEEE Transactions on Aerospace and Electronic Systems*, **38**, 2 (Apr. 2002), 553–569.
- [11] Keysight Technologies (Agilent), e-mail correspondence with Ping Zhou, Keysight Technologies, Customer Contact Center, P.O. Box 4026, Englewood, CO, USA, Jan. 2015.
- [12] Helton, J., Chen, C.-I. H., Lin, D. M., and Tsui, J. B. Y. FPGA-based 1.2 GHz bandwidth digital instantaneous frequency measurement receiver. In *Proceedings of 9th International Symposium on Quality Electronic Design*, San Jose, CA, 2008, 568–571.
- [13] Tsui, J. *Special Design Topics in Digital Wideband Receivers*. Boston, London: Artech House, 2010.
- [14] East, P. W. Fifty years of instantaneous frequency measurement. *IET Radar and Sonar Navigation*, **6**, 2 (2012), 112–122.
- [15] Pandolfi, C., Fitini, E., Gabrielli, G., Megna, E., and Zaccaron, A. Comparison of analog IFM and digital frequency measurement receivers for electronic warfare. In *Proceedings of the 7th European Radar Conference 2010*, Oct. 2010, 232–235.
- [16] Murthy, D. S. Real-time Hilbert transform and autocorrelation for digital wideband communication applications. M.S. thesis, Wright State University, Dayton, OH, 2008.
- [17] Lin, D. M., Liou, L. L., Benson, S., and Chen, C.-I. H. Mono-bit digital chirp receiver using mono-bit IFM (instantaneous frequency measurement) receiver as a core. In *Proceedings of the Aerospace and Electronics Conference*, Jul. 2011, 348–351.
- [18] Lopez-Risueno, G., Grajal, J., and Sanz-Osorio, A. Digital channelized receiver based on time-frequency analysis for signal interception. *IEEE Transactions on Aerospace and Electronic Systems*, **41**, 3 (2005), 879–898.

Stephen Ray Benson received the B.S. degree in computer engineering and the M.S.E.E. degree from Wright State University, Dayton, OH, in 2008 and 2010, respectively, where he is currently working toward the Ph.D. degree in electrical engineering. His primary research area is in the detection of high chirp rate short pulse duration nonlinear chirp signals.

Chien-In Henry Chen (S'89–M'89) received the Ph.D. degree in electrical engineering from the University of Minnesota, Minneapolis, in 1989. Since joining Wright State University in 1989, he has worked primarily in design and test of digital and mixed-signal RF ICs, VLSI/FPGA/GPU for real-time signal processors and ultra-wideband receivers, where he is currently a professor. He has written over 120 publications and has served as editor, associate editor, and technical committee member on numerous professional journals and conferences. He has advised 8 Ph.D. and 45 M.S. thesis students.

David M. Lin received his B.S.E.E. from Tatung Institute of Technology, Taiwan, in 1970; his M.S.E.E. and M.E.M.E. from Tennessee Technological University, Cookeville, TN, in 1977 and 1978, respectively; and his M.S.C.S. from Wright State University, Dayton, OH, in 1984. From 1979 to 1985, he was a software engineer at System Research Laboratories Inc., Dayton, OH. Since 1985, he has been an electronics engineer at the Air Force Research Laboratory (AFRL), Wright Patterson Air Force Base, OH. His work involves EW, radar, and global positioning system receivers. He has received 10 patents.

Lihyeh L. Liou (S'82–M'87–SM'95) received his B.S. degree in physics from National Tsing-Hua University, Hsin-Chu, Taiwan, in 1976; his M.S. degree in geophysics from National Taiwan University, Taipei, Taiwan, in 1978; and his Ph.D. degree in physics from University of Southern California, Los Angeles, in 1985. From 1985 to 1986, Dr. Liou was with Hewlett-Packard's Fort Collins, CO, Integrated Circuit Division. From 1987 to 1989, he was with Universal Energy System Inc., Dayton, OH. Since 1990, he has been with the AFRL, Wright-Patterson Air Force Base, Dayton, OH. He is presently working on signal processing-related topics, including digital beam forming and EW receiver algorithm development.